Check for updates

Received: 12 February 2020 | Revised: 24 June 2020 | Accepted: 26 June 2020

DOI: 10.1002/nbm.4374

RESEARCH ARTICLE

NMR IN BIOMEDICINE WILEY

Blood–brain barrier permeability measurement by biexponentially modeling whole-brain arterial spin labeling data with multiple T_2-weightings

Martin Schidlowski[1,2] | Markus Boland[2] | Theodor Rüber[1,3,4] | Tony Stöcker[2,5]

[1]Department of Epileptology, University of Bonn Medical Center, Bonn, Germany

[2]German Center for Neurodegenerative Diseases (DZNE), Bonn, Germany

[3]Epilepsy Center Frankfurt Rhine-Main, Department of Neurology, Goethe University Frankfurt, Frankfurt/Main, Germany

[4]Center for Personalized Translational Epilepsy Research (CePTER), Goethe University Frankfurt, Frankfurt/Main, Germany

[5]Department for Physics and Astronomy, University of Bonn, Bonn, Germany

Correspondence
Tony Stöcker, German Center for Neurodegenerative Diseases (DZNE), Venusberg-Campus 1, 53127 Bonn, Germany.
Email: tony.stoecker@dzne.de

Abstract

Blood–brain barrier (BBB) permeability assessment remains of ongoing interest in clinical practice and research. Transitions between intravascular (IV) and extravascular (EV) gray matter (GM) compartments may provide information regarding the microstructural status of the BBB. Due to different transverse relaxation times (T_2) of water protons in vessels and GM, it is possible to determine the compartment in which these protons are located. This work presents and investigates the feasibility of a simplified analytical approach for compartmentalizing the proportions of magnetically marked water protons into IV and EV GM components by biexponentially modeling T_2-weighted arterial spin labeling (ASL) data. Numerous model assumptions were used to stabilize the fit and achieve in vivo applicability. Particularly, transverse relaxation times of IV and EV water protons were determined from the analysis of two supporting T_2-weighted ASL measurements, utilizing a monoexponential signal model. This stabilized a two-parameter biexponential fit of ASL data with T_2 preparation (PLD = 0.9/1.2/1.5/1.8 s, TE_{T2Prep} = 0/30/40/60/80/120/160 ms), which thereby robustly provided estimates of the IV and EV compartment fractions. Experiments were conducted with three healthy volunteers in a 3 T scanner. Averaged over all subjects, the labeled water protons inherit $T_{2,IV}$ = 200 ± 18 ms initially and adapt $T_{2,EV}$ = 91 ± 2 ms with a longer retention time in cerebral structures. Accordingly, the EVlocated ASL signal fraction rises with increasing PLD from 0.31 ± 0.11 at the shortest PLD of 0.9 s to 0.73 ± 0.02 at the longest PLD of 1.8s. These results indicate a transition of the water protons from IV to EV space. The findings support the potential of biexponential modeling for compartmentalizing ASL spin fractions between IV and EV space. The novel integration of monoexponential parameter estimates stabilizes the two-compartment model fit, suggesting that this technique is suitable for robustly estimating the BBB permeability in vivo.

Abbreviations used: ASL, arterial spin labeling; ATT, arterial transit time; BBB, blood–brain barrier; BS, background suppression; BW, bandwidth; CBF, cerebral blood flow; CT pair, control-tag pair; ETL, echo train length; EV, extravascular; FA, flip angle; FOV, field of view; G, gradient; Gd, gadolinium; GM, gray matter; GRASE, gradient and spin echo; IV, intravascular; MLEV, Malcolm Levitt; NLLS, non-linear least squares; pCASL, pseudocontinuous arterial spin labeling; PE, phase encoding; PLD, postlabeling delay; PROT, protocol; RF, radio frequency; ROI, region of interest; SEG, segment; SNR, signal-to-noise ratio; TE, echo time; TR, repetition time.

Theodor Rüber and Tony Stöcker contributed equally to this work.

This is an open access article under the terms of the Creative Commons Attribution License, which permits use, distribution and reproduction in any medium, provided the original work is properly cited.
© 2020 The Authors. NMR in Biomedicine published by John Wiley & Sons Ltd

KEYWORDS
biexponential signal modeling, blood–brain barrier permeability measurement, ASL signal compartmentalization, T_2 mapping, T_2-weighted arterial spin labeling

1 | INTRODUCTION

Arterial spin labeling (ASL) is a non-invasive MRI technique using blood water molecules as an endogenous tracer.[1] In this method, arterial blood water protons are marked magnetically by inversion of the longitudinal magnetization component. The blood flows into cerebral structures where an exchange of water molecules takes place between intravascular (IV) and extravascular (EV) space, thereby crossing the semipermeable blood–brain barrier (BBB). The determination of BBB permeability is the subject of current research and, for instance, is examined using gadolinium (Gd)-containing contrast agents by detecting pathological passages of these injected molecules.[2] However, methodological disadvantages can result from the properties of the contrast agent molecules, including size, charge and hydrophilicity, which may influence and hinder BBB passage.[3] While ASL is used more frequently for perfusion measurements in scientific and clinical practice, permeability assessment has so far only been a subject of research. Here, various MRI techniques, models and potential clinical applications for analyzing the water exchange across the BBB have been suggested to overcome the aforementioned limitations.[4,5]

Those earlier studies have tried to exploit this benefit of ASL. Some approaches estimated the EV signal fraction or the water exchange rate, based on the suppression of IV signal and following comparison with unsuppressed reference measurements.[6,7] The suppression of IV signal was in this case achieved via diffusion weighting or vascular crushing gradients. Another method modeled global tissue extraction rate and BBB transitions by quantifying the venous ASL signal in the sagittal sinusi.e. outflowing arterially labeled spins.[4] Further studies have investigated signal allocation by applying T_2-weighted ASL data to a two-compartment model with numerous input and fit parameters.[8,9]

This work adopts, modifies and extends an approach to compartmentalize ASL data. The approach is based on previous studies, showing that IV and EV T_2 differ and T_2-weighted ASL signal proportions of both spaces can be separated.[8,9] However, T_2-based compartmentalization approaches have predominantly been able to make global statements within a region of interest (ROI) or have included complex models with many parameters that may lead to a poorly conditioned model inversion resulting in large error bounds. A promising concept has been demonstrated in animal studies, which builds on the biexponential modeling of ASL data.[10,11] Based on this idea, our study extends the approach to the human brain with modified and newly introduced processing steps and model assumptions: in order to obtain a robustly performing biexponential fit, we designed additional measurements for the modeling of IV and EV water proton T_2 relaxation times within a monoexponential model fit of ROI data. As shown, this novel combination of mono- and biexponential fitting techniques stabilizes the two-compartment modeling of the SNR-limited T_2-weighted ASL data to the point that the compartmentalization procedure becomes possible for human in vivo applications.

2 | MATERIALS AND METHODS

2.1 | Theory

The BBB is a membrane that forms a physiological barrier between IV blood and EV brain tissue and selectively enables substances which are transported by the blood to pass through it. This passage can occur by diffusion or through dedicated, active or passive, transport channels. Water molecules freely diffuse across this membrane and are also transported through aquaporin channels, with the latter being the faster mechanism. The water transport rate, which also is referred to as permeability, represents an approach to infer the functionality of the BBB.[5,11]

The effective transverse relaxation time T_2 depends on numerous factors. In particular, for blood water protons, it depends on the properties of the surrounding tissue, including the blood oxygenation level and hematocrit. Accordingly, the T_2 of water protons located in the arteries, veins, gray matter and white matter is different. An even more detailed segmentation into further compartments with characteristic T_2 times can be made.[12,13]

The two-compartment model simplifies the complex structure. It is assumed that the labeled water protons are located in the arterial compartment initially and directly pass into the cerebral tissue compartment. Consequently, only the transverse relaxation times of arterial blood and tissue water protons are considered.[8,14]

Subsequently, these assumptions are integrated into a strongly simplified biexponential model for the localization of arterially labeled water protons. Thereby, two compartments are considered to exist with two distinct transverse relaxation times. These are referred to as $T_{2,IV}$ for arterial water protons located inside the first compartment, the intravascular space, and $T_{2,EV}$ for those inside the second compartment, the extravascular cerebral gray matter tissue. Furthermore, it is assumed that there are equal water densities within both compartments and partial volume effects with white matter and CSF to be negligible. Additional model simplifications are the disregard of the blood oxygenation level, the hematocrit and a possible signal contribution of venous blood flow. These possibly affect the T_2 determination and biexponential compartmentalization.

10991492, 2020, 10, Downloaded from https://analyticalsciencejournals.onlinelibrary.wiley.com/doi/10.1002/nbm.4374 by Deutsches Zentrum Für Neurodeg, Wiley Online Library on [25/05/2023]. See the Terms and Conditions (https://onlinelibrary.wiley.com/terms-and-conditions) on Wiley Online Library for rules of use; OA articles are governed by the applicable Creative Commons License

2.2 | ASL sequence

An inhouse-developed pseudocontinuous arterial spin labeling (pCASL) sequence[15] (Figure 1) was extended by a T_2 preparation module prior to the GRASE readout. It enables the acquisition of multiple T_2-weightings, resulting in different echo times (TEs) and the acquisition of multiple postlabeling delays (PLDs). In order to separate IV and EV compartments from each other, a T_2-weighting, TE_{T2Prep}, with variable length is induced. The preparation module is made up of non-selective composite pulses which, depending on the preparation time, TE_{T2Prep}, are arranged in three different Malcolm Levitt (MLEV) cycling schemes with 4 (TE_{T2Prep} = 30/40 ms), 8 (TE_{T2Prep} = 60/80 ms) and 16 (TE_{T2Prep} = 120/160 ms) refocusing pulses.[16] This approach reduces off-resonance effects and compensates B_1 imperfections thus enabling more precise spin refocusing and improving transverse relaxation time estimates.[17,18]

2.3 | Acquisition protocol

The study consists of three separate scanning protocols (Table 1), named "monoexponential T_2 estimation protocols" $PROT_{IV}$ and $PROT_{EV}$ and "biexponential compartmentalization protocol" $PROT_{IV+EV}$ (Figure 2). The monoexponential T_2 estimation protocols are used for the analysis of intravascular ($PROT_{IV}$) and extravascular ($PROT_{EV}$) water proton T_2 values. The biexponential compartmentalization protocol ($PROT_{IV+EV}$) provides the input data for the compartmentalization of the ASL signal. In a first step, a preprocessing (described in section 2.5) is applied to the data of all protocols. Next, a monoexponential fit of the T_2 estimation protocols data is utilized to determine the T_2 for IV and EV water protons within GM. Results are then used as subject-specific input parameters for a biexponential fit of the more comprehensive biexponential compartmentalization protocol data to localize labeled spins.

2.4 | In vivo experiments

For the proof-of-concept study three healthy volunteers (two females, one male, aged 25 ± 2 years) were scanned on a Magnetom Trio 3T scanner (Siemens Healthineers, Erlangen, Germany) using a 32-channel head coil. All experiments were performed in accordance with the institutional review board of the medical faculty of the University of Bonn and prior written informed consent was obtained from the subjects. Following the auto-align scout, a time-of-flight scan was used to position the ASL labeling plane slightly inferior to the lower end of the cerebellum. This ensures

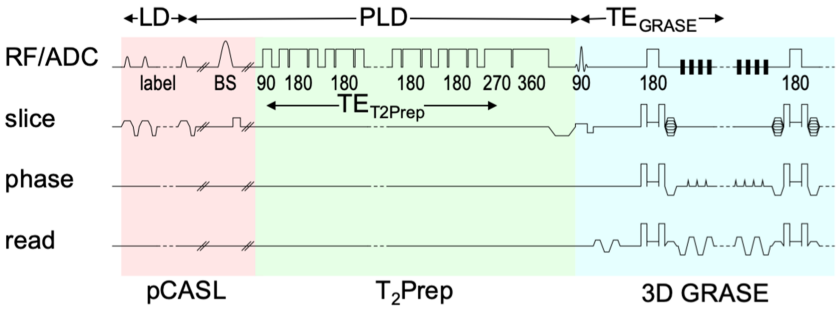

FIGURE 1 Diagram of T_2-prepared pCASL sequence. A WET presaturation of the imaging region is performed before pCASL labeling (not shown). Three background suppression (BS) pulses are timed to suppress static tissue signal. Only a single BS pulse is shown for clarity. The pulses may interrupt the labeling but not the T_2 preparation which is played out immediately before the 3D GRASE readout. In case of an interruption the label condition is changed between tag and control. In order to induce different T_2-weightings, TE_{T2Prep}, the preparation module is made up of non-selective composite pulses arranged in three different Malcolm Levitt (MLEV) cycling schemes with 4 (TE_{T2Prep} = 30/40 ms), 8 (TE_{T2Prep} = 60/80 ms) and 16 (TE_{T2Prep} = 120/160 ms) refocusing pulses as well as a composed 270°-360° tip-up pulse to compensate for off-resonance effects and B_1 imperfections. The pulse durations for the flip angles 90°/180°/270°/360° are 0.8/1.6/2.4/3.2 ms. There is an inter-echo spacing of 7.5 ms for TE_{T2Prep} = 30/60/120 ms, 10 ms for TE_{T2Prep} = 40/80/160 ms and the gap between the composite pulses takes 0.15 ms. For a simpler representation, only the shortest T_2 preparation is shown and dashed lines indicate further repetitions

10991492, 2020, 10, Downloaded from https://analyticalsciencejournals.onlinelibrary.wiley.com/doi/10.1002/nbm.4374 by Deutsches Zentrum Für Neurodeg, Wiley Online Library on [25/05/2023]. See the Terms and Conditions (https://onlinelibrary.wiley.com/terms-and-conditions) on Wiley Online Library for rules of use; OA articles are governed by the applicable Creative Commons License

TABLE 1 Acquisition protocol and ASL parameters. Calibration images M_0 are acquired with alternating orientation of PE polarity and distortion corrected using FSL's function topup. Additionally, a structural T_1-weighted image (0.8 mm isotropic) is measured. The scan times are 45 min 20 s for compartmentalization ASL data (6 MEAS/PLD/TE_{T2Prep}/SEG/CT pair), 1 min 15 s for corresponding calibration scans (2 MEAS/PE polarity), 5 min 38 s for T_2 estimation ASL data (6 MEAS/PLD/TE_{T2Prep}/BS condition/CT pair), 26 s for corresponding calibration scans (2 MEAS/PE polarity) and 6 min 32 s for T_1 scan resulting in a total scan time of 59 min 11 s. Explanations are given in the list of abbreviations.

	monoexponential T_2 estimation protocols ($PROT_{IV}$/$PROT_{EV}$)	**biexponential compartmentalization protocol ($PROT_{IV+EV}$)**
3D GRASE		
FOV	210 x 210 x 120 mm^3	210 x 210 x 120 mm^3
acquisition matrix	42 x 42 x24	70 x 70 x 30
resolution	5 x 5 x 5 mm^3	3 x 3 x 4 mm^3
TE_{GRASE}	16 ms	22.9 ms
PE	GRAPPA 2x	GRAPPA 2x
3D	1x SEG	2x SEG
BW	2588 Hz/Px	2551 Hz/Px
ETL	392 ms	355 ms
ASL		
LD	1.8 s	1.8 s
PLD	0.25 s	0.9/1.2/1.5/1.8 s
TE_{T2Prep}	0/30/40/60/80/120/160 ms	0/30/40/60/80/120/160 ms
TR	4.02 s	4.02 s
BS	on ($PROT_{IV}$) /off ($PROT_{EV}$)	on
M_0 calibration		
TR	6 s	6 s
ASL labeling	**common parameters**	
method	unbalanced	
G_{avg}	0.5 mT/m	
G_{max}	3.5 mT/m	
FA	34°	
RF duration	500 μs	
RF gap	660 μs	

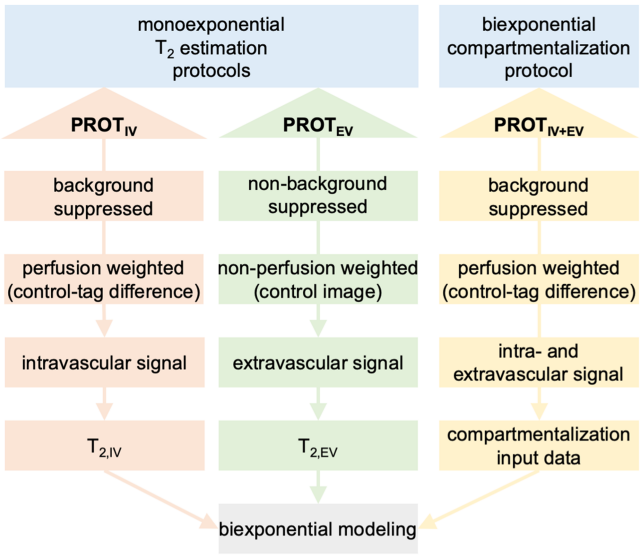

FIGURE 2 Overview of applied ASL protocols. The T_2 estimation protocols comprise two series: background suppressed and perfusion-weighted images (red) from series $PROT_{IV}$ are used for an analysis of intravascular $T_{2,IV}$ and non-background suppressed control images (green) from series $PROT_{EV}$ provide an approximation basis for extravascular $T_{2,EV}$. The compartmentalization protocol $PROT_{IV+EV}$ (yellow) provides the data for compartmentalization, which together with both T_2 estimates, are input for the biexponential modeling

10991492, 2020, 10, Downloaded from https://analyticalsciencejournals.onlinelibrary.wiley.com/doi/10.1002/nbm.4374 by Deutsches Zentrum Für Neurodeg, Wiley Online Library on [25/05/2023]. See the Terms and Conditions (https://onlinelibrary.wiley.com/terms-and-conditions) on Wiley Online Library for rules of use; OA articles are governed by the applicable Creative Commons License

blood water proton inversion in the basilar and the right and left internal carotid arteries. The acquisition protocols and ASL parameters are summarized in Table 1.

The scan protocol is based on the recommendations of the ISMRM consensus paper on ASL imaging[1] and a previous study.[15] The following ASL parameters were applied: unbalanced pCASL labeling, a labeling duration of 1.8 s (as a compromise between signal strength for T_2-weighting, acquisition time and SAR) and TE_{T2Prep} lengths of 0/30/40/60/80/120/160 ms. In order to achieve a steady state, two preparation scans were acquired and removed before data analysis. Calibration images were acquired with alternating orientation of phase-encoding (PE) polarity to allow for distortion correction.

Experiments for compartmentalization were performed with PLD=0.9/1.2/1.5/1.8 s to ensure sufficient time for compartment transitions of labeled spins. The resolution of the 3D GRASE readout was 3 x 3 x 4 mm^3 and each control-tag (CT) pair and readout segment (SEG) was measured six times for each PLD and each TE_{T2Prep}, resulting in a scan time of 45 min 20 s. Calibration images were acquired twice per segment and PE polarity (1 min 15 s). As a tradeoff between acquisition time (1x SEG) and signal-to-noise ratio (SNR), a larger voxel size of 5 mm^3 was used for the T_2 estimation scans. A reduced PLD of 0.25 s in these scans led to a measurement of the label shortly after arrival in cerebral structures. For the analysis of IV and EV T_2 under simplified model assumptions, two separate measurement series were included with background suppression (BS) enabled and disabled. Each perfusion-weighted volume (CT pair) acquisition was measured six times for each TE_{T2Prep}. The corresponding calibration images were measured twice per PE polarity, resulting in a total scan time of 6 min 32 s for the T_2 estimation protocols.

For registration purposes, an additional structural T_1-weighted image with an isotropic resolution of 0.8 mm was acquired (6 min 32 s).

The complete protocol, along with the calibration images and the structural scan, resulted in a total acquisition time of 59 min 11 s.

2.5 | Preprocessing

Preprocessing of online reconstructed data includes the application of toolboxes from FMRIB's Software Library.[19] For normalization, the T_1-weighted structural scan is processed with fsl_anat[20] to obtain a transform from structural to MNI space. The ASL image time series is motion-corrected with mcflirt[21] and distortion-corrected with topup[22] utilizing phase-reversed calibration scans. Pairwise subtraction yields perfusion-weighted images, which are averaged to create mean perfusion-weighted images

$$S_{\mathrm{ASL}}(\mathrm{PLD}, \mathrm{TE}_{\mathrm{T2Prep}}) = (M_{\mathrm{control}}(\mathrm{PLD}, \mathrm{TE}_{\mathrm{T2Prep}}) - M_{\mathrm{tag}}(\mathrm{PLD}, \mathrm{TE}_{\mathrm{T2Prep}}))/M_0 \tag{1}$$

for every PLD and TE_{T2Prep} separately. Subsequently, a brain mask is applied. The preprocessed ASL data and fsl_anat results are taken as input for oxford_asl[23] to calculate arterial transit times (ATT), cerebral blood flow (CBF), transformations from native to structural space and a GM mask. The latter is then applied to the preprocessed ASL data. Finally, the $PROT_{IV+EV}$ data are smoothed with a three-dimensional, 4.7 mm full width at half maximum, isotropic Gaussian kernel to reduce the random noise and increase the SNR for the subsequent modeling.[24,25]

2.6 | IV and EV monoexponential T_2 estimation

For the approximation of IV arterial water proton $T_{2,IV}$ and EV tissue water proton $T_{2,EV}$, data obtained from both T_2 estimation protocols $PROT_{IV}$ and $PROT_{EV}$ (Figure 2) are analyzed separately for each subject (not shown). Since it is challenging to quantify T_2 values on low SNR perfusion-weighted images,[26] the following assumptions are made.

Perfusion-weighted images are created from the background-suppressed series $PROT_{IV}$. Subsequently, a GM masking is performed and T_2 maps are generated. Due to BS and subtraction, the signal is largely free of static tissue, so that blood is dominant. Because of the short PLD, it is furthermore reasonable to assume that the spins are still predominantly located in the IV space. Therefore, the median T_2 of the obtained maps in this series approximately represents the IV $T_{2,IV}$.

In contrast to this, GM masking is also performed in the unsuppressed series $PROT_{EV}$, but T_2 maps are fitted from control images, which means that no differences are formed. The signal is almost PLD-independent and predominantly corresponds to the static GM, since neither BS nor difference formation are present. So, from the series $PROT_{EV}$ resulting median T_2 can be assigned to the EV GM compartment and may be referred to as EV $T_{2,EV}$.

In both approximations, T_2 maps are generated by applying a monoexponential non-linear least squares (NLLS) fit along the TE_{T2Prep}-axis utilizing the Python function curve_fit from the Scipy.Optimize library with the following model:

$$S_{\mathrm{ASL}}(\mathrm{PLD}, \mathrm{TE}_{\mathrm{T2Prep}}) = S_0(\mathrm{PLD}) \cdot e^{-\mathrm{TE}_{\mathrm{T2Prep}}/T_2}. \tag{2}$$

10991492, 2020, 10, Downloaded from https://analyticalsciencejournals.onlinelibrary.wiley.com/doi/10.1002/nbm.4374 by Deutsches Zentrum Für Neurodeg, Wiley Online Library on [25/05/2023]. See the Terms and Conditions (https://onlinelibrary.wiley.com/terms-and-conditions) on Wiley Online Library for rules of use; OA articles are governed by the applicable Creative Commons License

2.7 | Biexponential compartmentalization

The biexponential two-parameter model requires knowledge of the T_2 of IV and EV GM compartment. Both values are obtained for each subject within the previously described monoexponential T_2 estimations and taken as input parameters.

In order to separate the signal source into IV and EV space, and given the aforementioned assumptions, a simplified biexponential model

$$S_{\mathrm{ASL}}(\mathrm{PLD}, \mathrm{TE}_{\mathrm{T2Prep}}, \mathrm{TE}_{\mathrm{GRASE}}) = S_{\mathrm{IV}}(\mathrm{PLD}) \cdot e^{-\left(\mathrm{TE}_{\mathrm{T2Prep}} + \mathrm{TE}_{\mathrm{GRASE}}\right)/T_{2,\mathrm{IV}}} + S_{\mathrm{EV}}(\mathrm{PLD}) \cdot e^{-\left(\mathrm{TE}_{\mathrm{T2Prep}} + \mathrm{TE}_{\mathrm{GRASE}}\right)/T_{2,\mathrm{EV}}} \tag{3}$$

along $\mathrm{TE}_{\mathrm{T2Prep}}+\mathrm{TE}_{\mathrm{GRASE}}$ is applied to the preprocessed perfusion-weighted data of the compartmentalization protocol ($\mathrm{PROT}_{\mathrm{IV+EV}}$) scans (Table 1). S_{IV} and S_{EV} represent the signal magnitudes from IV and EV space, respectively. The fit is performed in a voxelwise manner, using a NLLS approach (curve_fit) for optimization. No additional bounds or constraints for S_{IV} and S_{EV} are used. Accordingly, the EV PLD-dependent S_{ASL} fraction f_{EV} is given by

$$f_{\mathrm{EV}}(\mathrm{PLD}) = S_{\mathrm{EV}}(\mathrm{PLD}) / (S_{\mathrm{IV}}(\mathrm{PLD}) + S_{\mathrm{EV}}(\mathrm{PLD})). \tag{4}$$

2.8 | Bulk ASL signal T_2 mapping

The monoexponential model from Equation 2 is also applied to the preprocessed perfusion-weighted compartmentalization protocol ($\mathrm{PROT}_{\mathrm{IV+EV}}$) data. T_2 maps obtained from this fit correspond to the mean T_2 of all ASL signal compartments within a voxel at a specific PLD.

2.9 | Compartment transition rate modeling

Water proton quantities separated into IV and EV compartments at different PLDs are used to model transition rates between both compartments. First, frequency histograms of the EV PLD-dependent S_{ASL} fraction f_{EV} are smoothed by applying a five bin-wide moving average filter for each PLD and subject. Subsequently, peak fractions $f_{\mathrm{EV,peak}}$ are detected. Along with the corresponding PLDs, these are applied to a linear model

$$f_{\mathrm{EV}}(\mathrm{PLD}) = k_{\mathrm{lin}} \cdot \mathrm{PLD} + b \tag{5}$$

and an exponential model

$$f_{\mathrm{EV}}(\mathrm{PLD}) = a \cdot \left(1 - e^{-k_{\mathrm{exp}} \cdot \mathrm{PLD}}\right) + b. \tag{6}$$

The slope parameter k_{lin} in the linear model and the parameter k_{exp} in the exponential model can be considered as measures reflecting water proton transition rates between both compartments.

3 | RESULTS

Perfusion-weighted GM-masked images of one subject are shown in Figure 3 for all PLDs and T_2-weightings of the compartmentalization protocol $\mathrm{PROT}_{\mathrm{IV+EV}}$. For the other two participants, these are provided in the supporting information (supplementary S1). The GM-SNR of the non-smoothed data ($\mathrm{SNR}_{\mathrm{GM}}$) is summarized in supplementary S2 for all subjects. It is considered to be sufficient for our analysis, even for the low SNR images with the longest PLD and the most pronounced T_2-weighting.

3.1 | IV and EV monoexponential T_2 estimation

The background-suppressed and perfusion-weighted series ($\mathrm{PROT}_{\mathrm{IV}}$) yields a subject-averaged $\bar{T}_{2,\mathrm{IV}} = 200 \pm 18\,\mathrm{ms}$ within GM-ROI, which is slightly higher than reported literature blood water proton T_2 values of 175-186 ms.[12,13] The T_2 estimation based on non-background-suppressed control images ($\mathrm{PROT}_{\mathrm{EV}}$) provides a subject-averaged $\bar{T}_{2,\mathrm{EV}} = 91 \pm 2\,\mathrm{ms}$, which is in good agreement with the literature reference T_2 of 71-110 ms.[27]

10991492, 2020, 10, Downloaded from https://analyticalsciencejournals.onlinelibrary.wiley.com/doi/10.1002/nbm.4374 by Deutsches Zentrum Für Neurodeg, Wiley Online Library on [25/05/2023]. See the Terms and Conditions (https://onlinelibrary.wiley.com/terms-and-conditions) on Wiley Online Library for rules of use; OA articles are governed by the applicable Creative Commons License

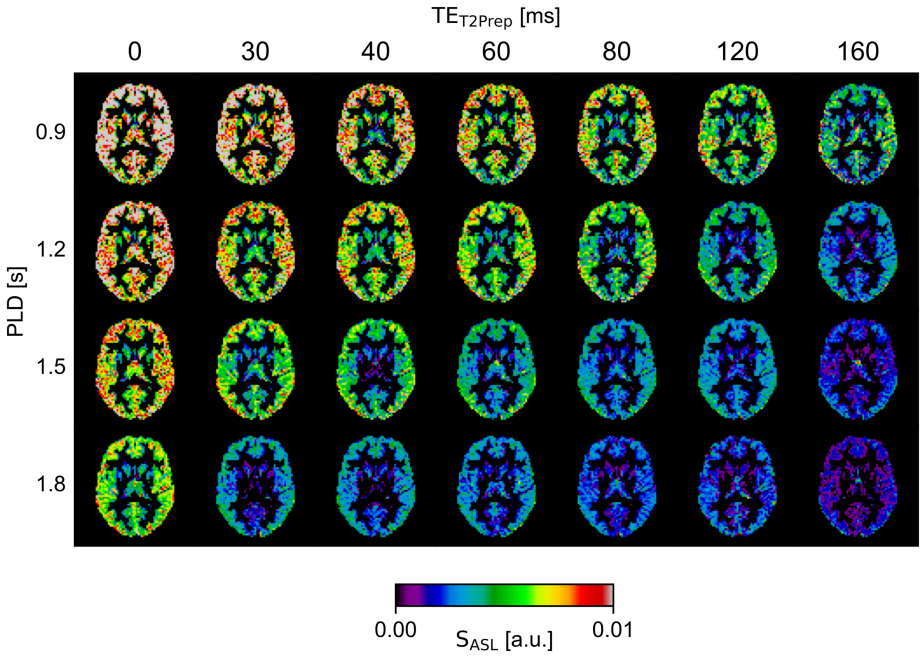

FIGURE 3 Mean perfusion-weighted ASL signal maps ($S_{ASL} = (M_{control}-M_{tag})/M_0$) in GM-ROI for all postlabeling delays (PLD = 0.9/1.2/1.5/1.8 s) and T_2 preparation times (TE_{T2Prep} = 0/30/40/60/80/120/160 ms) of one subject. The data are displayed in native space without smoothing

3.2 | Biexponential compartmentalization

Compartmentalization maps of exemplary slices for all PLDs are presented in Figure 4A. At short PLDs, the EV ASL signal fraction in the occipital lobe is small. An increase of f_{EV} with longer PLD can be appreciated in Figure 4A for all subjects. The frequency distributions of f_{EV} within the GM mask in Figure 5B support this trend. Quantified f_{EV} in GM-ROI as mean values for all subjects are 0.31 ± 0.11 at PLD = 0.9 s, increase to 0.52 ± 0.01 at PLD = 1.2 s and 0.66 ± 0.03 at PLD = 1.5 s, until they reach 0.73 ± 0.02 at PLD = 1.8 s. The standard error of f_{EV} determination $\sigma(f_{EV})$ is shown in the corresponding error maps (Figure 6A).

Instead of using subject-specific estimates as model input parameters, two additional compartmentalizations with fixed values of $T_{2,IV,181}$ = 181 ms for the IV and $T_{2,EV,91}$ = 91 ms respectively $T_{2,EV,68}$ = 68 ms for the EV compartment for all subjects provide frequency distributions of $f_{EV,181/91}$ and $f_{EV,181/68}$, which are shown in Figure 5C,D.

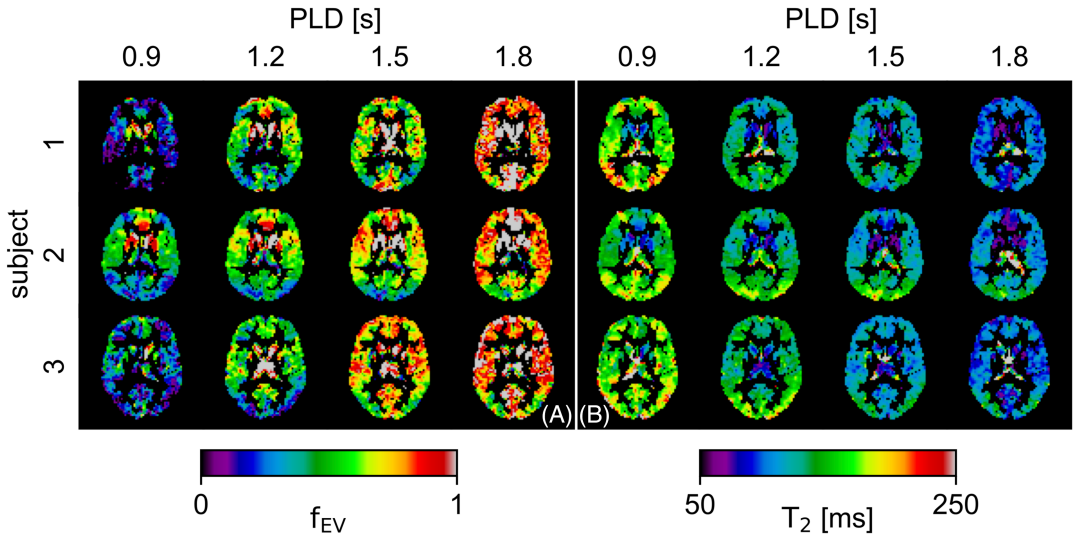

FIGURE 4 (A) Extravascular ASL signal fraction f_{EV}, and (B) T_2 maps in GM-ROI. Analysis results of all subjects are shown in native space for all postlabeling delays (PLD = 0.9/1.2/1.5/1.8 s). Small f_{EV} at the shortest PLD lead to signal drops in the displayed maps

10991492, 2020, 10, Downloaded from https://analyticalsciencejournals.onlinelibrary.wiley.com/doi/10.1002/nbm.4374 by Deutsches Zentrum Für Neurodeg, Wiley Online Library on [25/05/2023]. See the Terms and Conditions (https://onlinelibrary.wiley.com/terms-and-conditions) on Wiley Online Library for rules of use; OA articles are governed by the applicable Creative Commons License

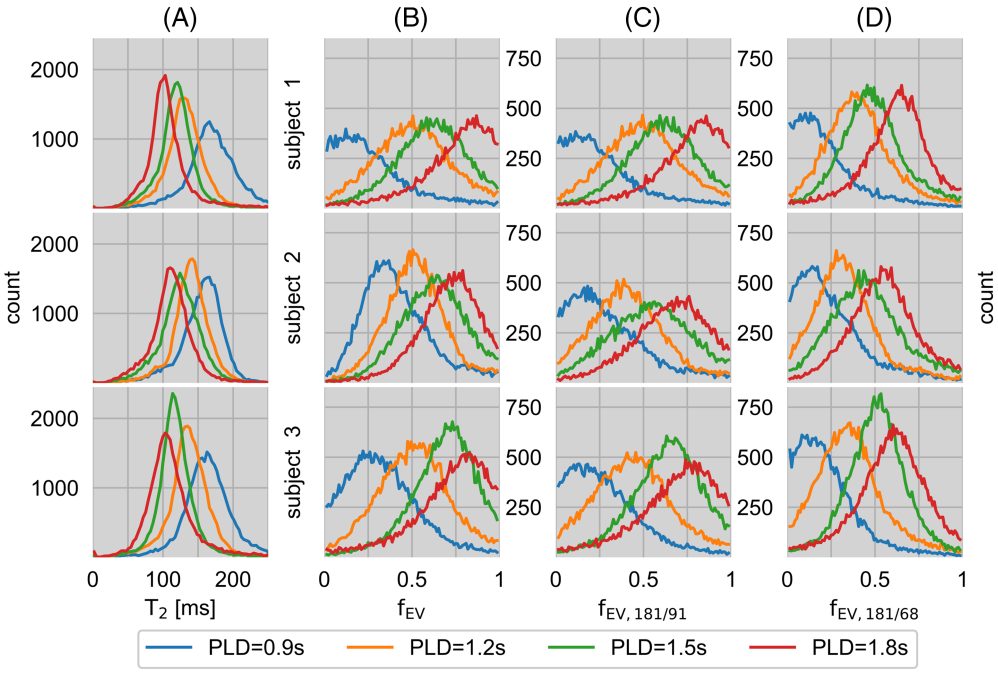

FIGURE 5 (A) Frequency distributions of T_2 relaxation times of the ASL signal and estimated EV ASL signal fractions in GM-ROI for all postlabeling delays (PLD = 0.9/1.2/1.5/1.8 s): (B)f_{EV} by usingsubject-specific $T_{2,IV}$ and $T_{2,EV}$, (C) $f_{EV,181/91}$ by applying fixed literature values $T_{2,IV,181}$ = 181 ms and $T_{2,EV,91}$ = 91 ms, and (D) $f_{EV,181/68}$ based on fixed literature values $T_{2,IV,181}$ = 181 ms and a shorter $T_{2,EV,68}$ = 68 ms. The decrease of T_2 relaxation time with rising PLD indicates that the labeled water protons adopt EV T_2 and are increasingly located in the EV compartment

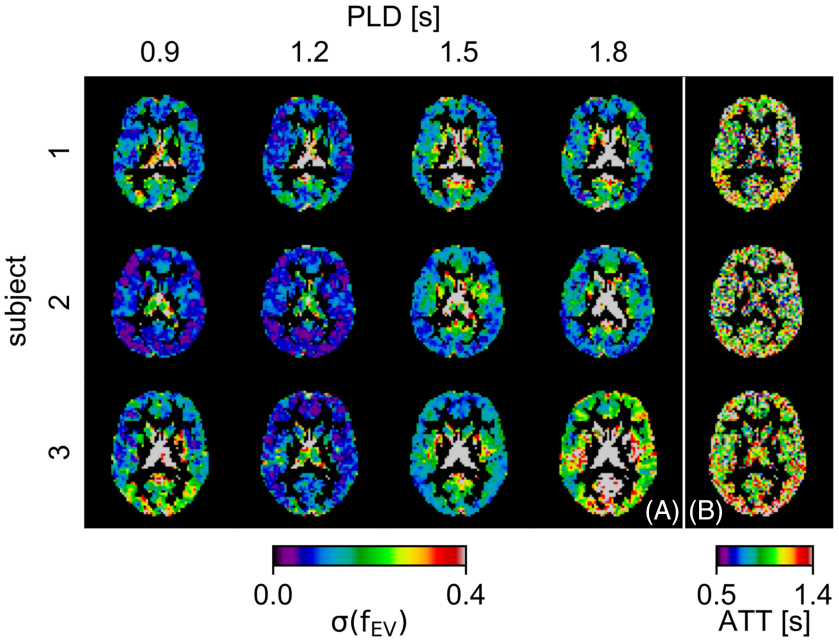

FIGURE 6 (A) EV ASL signal fraction standard error maps $\sigma(f_{EV})$ calculated from the fit parameter estimate variances and (B) arterial transit times (ATT) in GM-ROI. ATT-related information in FSL's BASIL setup are a variable arterial arrival time, an initial bolus arrival time of 1.3 s and a fixed bolus duration. Analysis results of all subjects are shown in native space for all postlabeling delays (PLD = 0.9/1.2/1.5/1.8 s)

3.3 | Bulk ASL signal T_2 mapping

T_2 maps of the perfusion-weighted signal within the GM-ROI are shown in Figure 4B for all PLDs. T_2 is prolonged in the occipital lobe, which is especially dominant at shorter PLDs. The region of prolonged T_2 values matches an area of longer ATTs in Figure 6B. There is a variance in T_2 between cerebral structures at different PLDs. An obvious trend of an overall decreasing T_2 with increasing PLD can be clearly observed in the frequency distributions in Figure 5A.

3.4 | Compartment transition rate modeling

The temporal dynamics of the EV fraction estimation are visible in the PLD course of the f_{EV} histograms and the detected peak fractions ($f_{EV,peak}$) in Figure 7A. Linear and biexponential modeling results are presented in Figure 7B for all subjects. The subject-averaged parameters of interest are k_{lin} = 0.62 ± 0.15 s^{-1} for the linear and k_{exp} = 0.88 ± 0.56 s^{-1} for the exponential model.

10991492, 2020, 10, Downloaded from https://analyticalsciencejournals.onlinelibrary.wiley.com/doi/10.1002/nbm.4374 by Deutsches Zentrum Für Neurodeg, Wiley Online Library on [25/05/2023]. See the Terms and Conditions (https://onlinelibrary.wiley.com/terms-and-conditions) on Wiley Online Library for rules of use; OA articles are governed by the applicable Creative Commons License

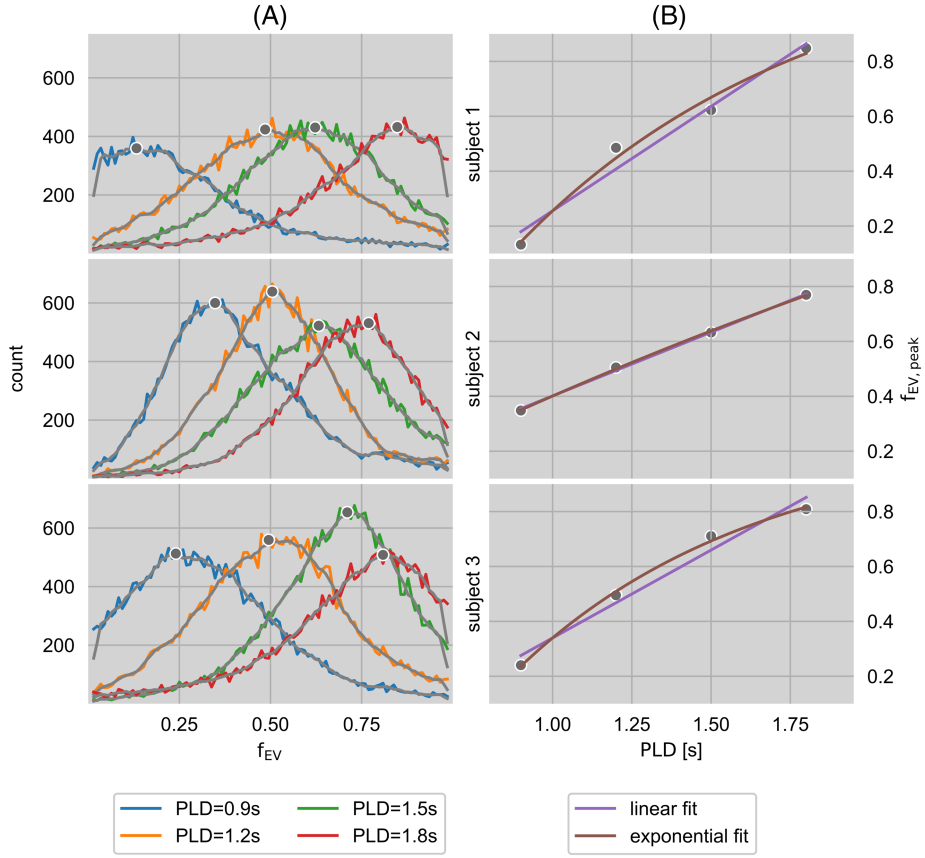

FIGURE 7 (A) Frequency distributions of estimated EV ASL signal fractions f_{EV} in GM-ROI for all postlabeling delays (PLD = 0.9/1.2/1.5/1.8 s) by using subject-specific $T_{2,IV}$ and $T_{2,EV}$, moving average filter smoothed data (gray) and detected peaks $f_{EV,peak}$. (B) Transition dynamic modeling by considering a linear (purple, see Equation 5) and an exponential (brown, see Equation 6) approach

4 | DISCUSSION

In this proof-of-concept study, we present an analytical approach to assess BBB permeability by compartmentalizing the proportions of labeled spins from T_2-prepared pCASL data into IV and EV GM components, which is possible because of different transverse relaxation times (T_2) of water protons in both modeled compartments. The SNR of T_2- and perfusion-weighted signal and the limited number of T_2-weightings make it unfeasible to accurately estimate compartment fractions and relaxation times from a combined model. Such a biexponential four-parameter fit failed entirely with our data (see supplementary S3). A better fit would require more repetitions as well as an increase and extended coverage of T_2-weightings, which results in unfeasible long scan protocols.[28] Even then accurate estimates are difficult to achieve, since multiexponential fitting is in general an ill-posed inverse problem.[26] However, the problem is no longer ill-posed if the exponential time constants are known beforehand. Therefore, in order to perform a stable fit and obtain a method that is applicable in vivo, we have combined mono- and biexponential two-parameter fitting techniques with approaches of ASL signal source allocation. Assuming monoexponential IV and EV signal decays in two appropriately designed supporting measurements, the feasibility of a compartmentalization was demonstrated in three subjects using seven different T_2-weightings within a total acquisition time of less than 1 hour. To the knowledge of the authors, it has never previously been shown that the preceding compartment parameter approximation based on a simplified monoexponential model stabilizes the two-compartment modeling of the SNR-limited T_2-weighted ASL human data.

Our results show a distinct dynamic in the transverse relaxation times: labeled water protons inherit $T_{2,IV}$ initially and adapt shorter $T_{2,EV}$ over time.[8] This progress indicates the transition of these protons from IV into EV space.[7] Thereby, these pass the BBB, which is a central assumption in the presented compartmentalization concept.[29] Consistently, the obtained mean EV compartmentalization fraction f_{EV} in GM-ROI averaged over all subjects is 0.31 ± 0.11 at the shortest PLD = 0.9 s. It increases to 0.52 ± 0.01 at a longer PLD = 1.2 s and 0.66 ± 0.03 at PLD = 1.5 s until a fraction of 0.73 ± 0.02 is reached at the longest PLD = 1.8 s. This ascending course with PLD supports the hypothesis of a BBB transition of labeled spins. However, an increasing contribution of non-exchanged, backflowing labeled venous spins with a shorter T_2 also cannot be excluded. With respect to differences in brain regions, bulk T_2 mapping shows higher values in the occipital lobe at shorter PLDs. This is presumably caused by CSF signal contributions, along with prolonged arterial transit times in this area.[30,31] Consistent with characteristic regional ATTs, f_{EV} results are remarkably lower in the occipital lobe. Therefore, these could also be linked to later arriving label, causing a possible underestimation of the EV signal component due to reduced ASL signal at short PLDs.[31,32] This is reflected by enlarged occipital compartmentalization uncertainties relative to other regions in two subjects, which are especially dominant at PLD = 0.9 s. A possibility for considering this influence consists of a PLD- and ATT-dependent masking to ensure that the compartmentalization is only performed for sufficiently large signal. Comparatively rapid

10991492, 2020, 10, Downloaded from https://analyticalsciencejournals.onlinelibrary.wiley.com/doi/10.1002/nbm.4374 by Deutsches Zentrum Für Neurodeg, Wiley Online Library on [25/05/2023]. See the Terms and Conditions (https://onlinelibrary.wiley.com/terms-and-conditions) on Wiley Online Library for rules of use; OA articles are governed by the applicable Creative Commons License

transitions into EV space tend to occur in the temporal lobes. Relative to this, labeled spins in the frontal lobe leave the IV space delayed. A largely balanced f_{EV} distribution in the GM structures is present at the longest PLD of 1.8 s. Likewise, these transition patterns correspond with known ATT dynamics.[30]

Several observations can be made: compartmentalization results show the increase of f_{EV} with retention time of labeled water protons in cerebral structures.[33] Also, the left–right symmetry in both hemispheres suggests balanced BBB transitions in all three subjects. Except for the shortest PLD, there is even good quantitative inter-subject agreement in the temporal course of f_{EV}, as it can be seen in the progression of the related frequency distributions (Figure 5B-D).

The transitions of water molecules between both compartments reflect the regular transport via aquaporin channels or by diffusion. Our hypothesis is that, depending on the BBB breakdown extent, this water permeability may also be sensitive to reflect the permeability of larger molecules. A related assessment is conceivable by comparing the f_{EV} maps (e.g. between healthy and diseased tissue, hemispheres or different PLDs). Another approach is the modeling of exchange times. Therefore, a three-compartment model including the capillary level and related capillary transit times would lead to more sophisticated approximations,[29] but it might be limited by SNR and the PLD sampling range. To still obtain an estimate, the global trend of the transition dynamics is modeled in two ways (Figure 7). A suspected saturation effect of the labeled water proton exchange cannot be demonstrated within the biexponential model. This could be caused by the narrow range of time points that characterize a linear regime. Transition dynamics derived from the linear model show comparable values in all three subjects and imply a relatively slower exchange in subject 2.

The major advantage of the presented method is IV and EV spin compartmentalization resolved at voxel level based on complete non-invasive[34] ASL data. Additionally, comparing our approach to BBB permeability mapping methods based on contrast agents, water molecules may provide a less hindered BBB passage than large contrast agent molecules. Moreover, there is no need for further measurements with signal-crushing or diffusion-weighting gradients.[35] Common ASL quantities, such as ATT and CBF, can still be calculated from the acquired data. The main advantage of the concept is the fit stabilization based on external $T_{2,IV}$ and $T_{2,EV}$ estimates. Here, we propose fast additional scans, which only take 10% of the total acquisition time and provide subject-specific fit parameters. A benefit of the modeling approach is its compact processing and analysis complexity, which keeps erroneous variables to a minimum and simplifies implementation.

In order to achieve a stable fit, both the determination of the model input T_2 values and the biexponential compartmentalization approach include strong simplifications and assumptions which are limiting factors: the presence of two compartments of equal water densities is assumed. Partial volume effects with white matter and CSF as well as an impact of venous blood are regarded as negligible. Furthermore, the blood oxygenation level and hematocrit are not considered, whereby the latter could even lead to a gender dependence in the arterial blood water proton T_2 values.[36]

The main assumption in our approach, which also has to be considered as a limiting factor, is the knowledge of T_2 values for IV and EV water protons in GM. They are obtained from monoexponential T_2 fitting of short PLD labeled and unlabeled acquisitions, respectively. These values are essential for compartmentalization and specify the quality, contrast and ultimately the differentiability between both compartments. Inevitably, the aforementioned assumptions and simplifications lead to inaccuracies in the determination of the T_2 values and also in the biexponential modeling. In our simplified approximation, $T_{2,EV}$ fits literature estimates better while $T_{2,IV}$ shows deviations.[12,13,27] The latter might be caused by physiological and subject-specific factors as well as different blood extravasation levels, which are particularly dominant at short PLDs and do not affect data for $T_{2,EV}$ estimation.[1] The increased uncertainty of the obtained $T_{2,IV}$ might also be attributed to the lower SNR of IV signal compared with total GM. This reduction is also caused by non-suppressed static tissue signal remaining in these data. Furthermore, individual vessels are not distinguished, in which the degree of blood oxygenation has a particularly strong effect on T_2. Altogether, we consider our approximation results to be in good agreement with literature values resulting from dedicated studies particularly designed for T_2 determination.[12,13,27] Even though $T_{2,EV}$ is in accordance with the literature, a lengthening of the cortical $T_{2,EV}$ due to partial volume effects with CSF cannot be excluded. Especially at longer TE_{T2Prep} the fraction of CSF would become more prominent. Along with known increased iron depositions in deep GM structures, this encourages a compartmentalization with a shorter time $T_{2,EV,68}$ (Figure 5D).[27] Therefore, two additional compartmentalizations were performed for all subjects using fixed literature values instead of subject-specific values. The corresponding frequency distributions are shown in Figure 5C,D. The results are largely comparable with slight shifts and width variations of the distribution peaks, which suggests the use of universal fit input parameters to be a practicable option. However, the results also show a dependence on the selected transverse relaxation times. Moreover, a modeling based on fixed input parameters may not fit well in subjects who deviate from the assumed norm. Particularly in those cases and as our approach increases the measurement time only slightly, the application of subject-specific values may be advantageous.

The in vivo applicable scan time limits the parameters, which can be acquired within a single session. In particular, a greater coverage of TEs would allow for more accurate fitting and probably further improve the compartmentalization quality.[10,26] The standard error of f_{EV} determination based on study protocol TEs is shown in Figure 6A. The simplifications stated above lead to further limitations, as for instance the approach does not account for the fact that blood oxygen level directly impacts water proton T_2 relaxation time.[12,13] This results in biased fraction estimates. However, the bias can be assumed to be constant throughout the measurements, so that it is reasonable to compare f_{EV} within the proposed method.

Based on the results of this proof-of-concept study, further investigations are needed. In particular, animal studies would allow more complex protocols, which could be applied to investigate animal models of BBB disorders.[37] Another promising approach would be to apply the method in

10991492, 2020, 10, Downloaded from https://analyticalsciencejournals.onlinelibrary.wiley.com/doi/10.1002/nbm.4374 by Deutsches Zentrum Für Neurodeg, Wiley Online Library on [25/05/2023]. See the Terms and Conditions (https://onlinelibrary.wiley.com/terms-and-conditions) on Wiley Online Library for rules of use; OA articles are governed by the applicable Creative Commons License

patients with a known BBB dysfunction such as brain tumors,[38] or to induce temporary BBB permeability change in healthy subjects with transcranial magnetic stimulation.[39]

With regard to future clinical applications, a shorter scan protocol would be required. For that purpose, the number of PLDs could be reduced: the BBB transition dynamics can already be studied by contrasting f_{EV} at only two PLDs instead of four. This corresponds to the measurement of only two f_{EV} data series in Figure 5B. Depending on the selected PLDs, it could halve the measurement time of the extensive $PROT_{IV+EV}$ compartmentalization data. Even a single PLD could be adequate for intra-subject comparisons (e.g. pre- and posttreatment). A further possibility to shorten the acquisition is to reduce the number of measurement repetitions used for data averaging. For this purpose, a subsampling of the data was performed. The biexponential modeling included all T_2-weightings and was based on a single measurement per PLD up to the mean data of the complete dataset (supplementary S4A). The associated standard errors seem to stabilize at an average of four individual measurements for all PLDs (supplementary S4B). This corresponds to a reduction of the compartmentalization data acquisition length by one third. Presently, no specific protocols can be recommended. Optimal values may vary with the study objective and likely are related to the subject group, which remains to be explored.[1,40,41] The combined reduction of acquired PLDs and averages would substantially reduce the measurement time and thereby clearly increase the clinical relevance of the proposed method.

As a consequence of the stated limitations and inaccuracies, the presented approach does not obtain exact permeabilities of the BBB. Nevertheless, it provides an opportunity to estimate intra- and extravascular water pool fractions. This might be of interest, in particular due to missing alternative non-invasive BBB assessment techniques.[4,7,33] The plausible results obtained within this proof-of-concept study suggest that this method has the potential to be used in future applications. At present, it may be especially suitable for studying whole-brain or at least large-scaled BBB disorders. The mapping accuracy needs to be investigated in future studies. In summary, we conclude that biexponential ASL modeling is a promising approach to non-invasively[34] investigate the status of the BBB in humans, which remains of ongoing interest in the research of numerous pathologies like Alzheimer's disease, multiple sclerosis and brain tumors.[38,42,43]

ACKNOWLEDGEMENT

Open access funding enabled and organized by Projekt DEAL.

ORCID

Martin Schidlowski https://orcid.org/0000-0003-4268-9291

Tony Stöcker https://orcid.org/0000-0002-8946-9141

REFERENCES

1. Alsop DC, Detre JA, Golay X, et al. Recommended implementation of arterial spin-labeled perfusion MRI for clinical applications: A consensus of the ISMRM perfusion study group and the European consortium for ASL in dementia. *Magn Reson Med.* 2014;73:102-116.
2. Heye AK, Culling RD, C. Valdés Hernández M del, et al. Assessment of bloodbrain barrier disruption using dynamic contrast-enhanced MRI. A systematic review. *NeuroImage Clin.* 2014;6:262-274.
3. Veiseh O, Sun C, Fang C, et al. Specific targeting of brain tumors with an optical/magnetic resonance imaging nanoprobe across the blood-brain barrier. *Cancer Res.* 2009;69:6200-6207.
4. Lin Z, Li Y, Su P, et al. Non-contrast MR imaging of blood-brain barrier permeability to water. *Magn Reson Med.* 2018;80:1507-1520.
5. Dickie BR, Parker GJM, Parkes LM. Measuring water exchange across the blood-brain barrier using MRI. *Prog Nucl Magn Reson Spectrosc.* 2020;116:19-39.
6. Lawrence KSS, Owen D, Wang DJJ. A two-stage approach for measuring vascular water exchange and arterial transit time by diffusion-weighted perfusion MRI. *Magn Reson Med.* 2011;67:1275-1284.
7. Wells JA, Lythgoe MF, Choy M, Gadian DG, Ordidge RJ, Thomas DL. Characterizing the origin of the arterial spin labelling signal in MRI using a multiecho acquisition approach. *J Cereb Blood Flow Metab.* 2009;29:1836-1845.
8. Liu P, Uh J, Lu H. Determination of spin compartment in arterial spin labeling MRI. *Magn Reson Med.* 2010;65:120-127.
9. Gregori J, Schuff N, Kern R, et al. T2-based arterial spin labeling measurements of blood to tissue water transfer in human brain. *J Magn Reson Imaging.* 2012;37:332-342.
10. Wells JA, Siow B, Lythgoe MF, et al. Measuring biexponential transverse relaxation of the ASL signal at 9.4 T to estimate arterial oxygen saturation and the time of exchange of labeled blood water into cortical brain tissue. *J Cereb Blood Flow Metab.* 2012;33:215-224.
11. Ohene Y, Harrison IF, Nahavandi P, et al. Non-invasive MRI of brain clearance pathways using multiple echo time arterial spin labelling: An aquaporin-4 study. *Neuroimage.* 2019;188:515-523.
12. Li W, Zijl PCM. Quantitative theory for the transverse relaxation time of blood water. *NMR Biomed.* 2020;33(5):e4207.
13. Chen JJ, Pike GB. Human whole blood T2 relaxometry at 3 Tesla. *Magn Reson Med.* 2009;61:249-254.
14. Hales PW, Clark CA. Combined arterial spin labeling and diffusion-weighted imaging for noninvasive estimation of capillary volume fraction and permeability-surface product in the human brain. *J Cereb Blood Flow Metab.* 2012;33:67-75.
15. Boland M, Stirnberg R, Pracht ED, et al. Accelerated 3D-GRASE imaging improves quantitative multiple post labeling delay arterial spin labeling. *Magn Reson Med.* 2018;80:2475-2484.
16. Levitt MH, Freeman R, Frenkiel T. Broadband heteronuclear decoupling. , et al. *J Magn Reson.* 1982;47:328-330.
17. Schmid S, Teeuwisse WM, Lu H, van Osch MJP. Time-efficient determination of spin compartments by time-encoded pCASL T2-relaxation-under-spin-tagging and its application in hemodynamic characterization of the cerebral border zones. *Neuroimage.* 2015;123:72-79.

10991492, 2020, 10, Downloaded from https://analyticalsciencejournals.onlinelibrary.wiley.com/doi/10.1002/nbm.4374 by Deutsches Zentrum Für Neurodeg, Wiley Online Library on [25/05/2023]. See the Terms and Conditions (https://onlinelibrary.wiley.com/terms-and-conditions) on Wiley Online Library for rules of use; OA articles are governed by the applicable Creative Commons License

18. Liu C-Y, Wieben O, Brittain JH, Reeder SB. Improved delayed enhanced myocardial imaging with T2-Prep inversion recovery magnetization preparation. *J Magn Reson Imaging*. 2008;28:1280-1286.
19. Smith SM, Jenkinson M, Woolrich MW, et al. Advances in functional and structural MR image analysis and implementation as FSL. *Neuroimage*. 2004;23:S208-S219.
20. Anatomical Processing Script: fsl_anat (BETA version). FMRIB Software Library Website, Oxford, UK. https://fsl.fmrib.ox.ac.uk/fsl/fslwiki/fsl_anat [].
21. Jenkinson M, Bannister P, Brady M, Smith S. Improved optimization for the robust and accurate linear registration and motion correction of brain images. *Neuroimage*. 2002;17:825-841.
22. Andersson JLR, Skare S, Ashburner J. How to correct susceptibility distortions in spin-echo echo-planar images: Application to diffusion tensor imaging. *Neuroimage*. 2003;20:870-888.
23. Chappell MA, Groves AR, Whitcher B, Woolrich MW. Variational Bayesian inference for a nonlinear forward model. *IEEE Trans Signal Process*. 2009;57:223-236.
24. Triantafyllou C, Hoge RD, Wald LL. Effect of spatial smoothing on physiological noise in high-resolution fMRI. *Neuroimage*. 2006;32:551-557.
25. Tabelow K, Piëch V, Polzehl J, Voss HU. High-resolution fMRI: Overcoming the signal-to-noise problem. *J Neurosci Methods*. 2009;178:357-365.
26. Istratov AA, Vyvenko O. Exponential analysis in physical phenomena. *Rev Sci Instrum*. 1999;70:1233-1257.
27. Lu H, Nagae-Poetscher LM, Golay X, Lin D, Pomper M, van Zijl PCM. Routine clinical brain MRI sequences for use at 3.0 Tesla. *J Magn Reson Imaging*. 2005;22:13-22.
28. Haller S, Zaharchuk G, Thomas DL, Lovblad KO, Barkhof F, Golay X. Arterial spin labeling perfusion of the brain: emerging clinical applications. *Radiology*. 2016;281:337-356.
29. K-I L, Zhu X, Hylton N, et al. Four-phase single-capillary stepwise model for kinetics in arterial spin labeling MRI. *Magn Reson Med*. 2005;53:511-518.
30. MacIntosh BJ, Filippini N, Chappell MA, et al. Assessment of arterial arrival times derived from multiple inversion time pulsed arterial spin labeling MRI. *Magn Reson Med*. 2010;63:641-647.
31. MacIntosh BJ, Swardfager W, Robertson AD, et al. Regional cerebral arterial transit time hemodynamics correlate with vascular risk factors and cognitive function in men with coronary artery disease. *Am J Neuroradiol*. 2014;36:295-301.
32. Hernandez-Garcia L, Lahiri A, Schollenberger J. Recent progress in ASL. *Neuroimage*. 2019;187:3-16.
33. He X, Raichle ME, Yablonskiy DA. Transmembrane dynamics of water exchange in human brain. *Magn Reson Med*. 2011;67:562-571.
34. Essig M, Shiroishi MS, Nguyen TB, et al. Perfusion MRI: the five most frequently asked technical questions. *Am J Roentgenol*. 2013;200:24-34.
35. Shao X, Ma SJ, Casey M, et al. Mapping water exchange across the blood-brain barrier using 3D diffusion-prepared arterial spin labeled perfusion MRI. *Magn Reson Med*. 2018;81:3065-3079.
36. Murphy WG. The sex difference in haemoglobin levels in adults mechanisms, causes, and consequences. *Blood Rev*. 2014;28:41-47.
37. Zhao B, Chen Y, Liu J, et al. Blood-brain barrier disruption induced by diagnostic ultrasound combined with microbubbles in mice. *Oncotarget*. 2018;9:4897-4914.
38. Arvanitis CD, Ferraro GB, Jain RK. The bloodbrain barrier and bloodtumour barrier in brain tumours and metastases. *Nature Reviews Cancer*. 2019;20(1):26-41.
39. Vazana U, Veksler R, Pell GS, et al. Glutamate-mediated blood-brain barrier opening: implications for neuroprotection and drug delivery. *J Neurosci*. 2016;36:7727-7739.
40. Kilroy E, Apostolova L, Liu C, Yan L, Ringman J, Wang DJJ. Reliability of two-dimensional and three-dimensional pseudo-continuous arterial spin labeling perfusion MRI in elderly populations: Comparison with 15o-water positron emission tomography. *J Magn Reson Imaging*. 2014;39:931-939.
41. Wang DJJ, Alger JR, Qiao JX, et al. Multi-delay multi-parametric arterial spin-labeled perfusion MRI in acute ischemic stroke comparison with dynamic susceptibility contrast enhanced perfusion imaging. *NeuroImage Clin*. 2013;3:1-7.
42. Shimizu F, Nishihara H, Kanda T. Bloodbrain barrier dysfunction in immuno-mediated neurological diseases. *Immun Med*. 2018;41:120-128.
43. Sweeney MD, Sagare AP, Zlokovic BV. Bloodbrain barrier breakdown in alzheimer disease and other neurodegenerative disorders. *Nat Rev Neurol*. 2018;14:133-150.

SUPPORTING INFORMATION

Additional supporting information may be found online in the Supporting Information section at the end of this article.

How to cite this article: Schidlowski M, Boland M, Rüber T, Stöcker T. Blood–brain barrier permeability measurement by biexponentially modeling whole-brain arterial spin labeling data with multiple T_2-weightings. *NMR in Biomedicine*. 2020;33:e4374. https://doi.org/10.1002/nbm.4374

10991492, 2020, 10, Downloaded from https://analyticalsciencejournals.onlinelibrary.wiley.com/doi/10.1002/nbm.4374 by Deutsches Zentrum Für Neurodeg, Wiley Online Library on [25/05/2023]. See the Terms and Conditions (https://onlinelibrary.wiley.com/terms-and-conditions) on Wiley Online Library for rules of use; OA articles are governed by the applicable Creative Commons License